CHEMISTRY
A EUROPEAN JOURNAL

Heteroditopic Ligand Accommodating a Fused Phenanthroline and a Schiff Base Cavity as Molecular Spacer in the Study of Electron and Energy Transfer

Yann Pellegrin,[a] Annamaria Quaranta,[b, c] Pierre Dorlet,[a] Marie France Charlot,[a] Winfried Leibl,*[b] and Ally Aukauloo*[a]

Abstract: The synthesis and characterisation of the heteroditopic ligand *N*,*N*′-bis(3,5-di-*tert*-butylsalicylidene)-5,6-(1,10-phenanthroline)diamine ($DPSalH_2$) bearing a phenanthroline and a bis(salicylidene)diimine cavity are reported. This versatile ligand combines two of the most widely used ligands in coordination chemistry. Sequential metallation of the phenanthroline end with Ru^{II} and the salophenic cavity with Cu^{II} is described. Electrochemical behaviour of the supramolecular complexes $[Ru(bpy)_2(DPSalH_2)]^{2+}$ and $[Ru(bpy)_2(DPSalCu)]^{2+}$ are analysed in connection with UV/Vis and EPR spectroscopy. The data for the one-electron-reduced species and the singly oxidised species of the binuclear Ru^{II}–Cu^{II} complex confirmed the formation of metalloradical complexes. Density functional calculations on the free ligand and the copper-only complex indicate in both cases that the HOMOs and LUMOs are developed on the Schiff base cavity with minor contributions on the bipyridine end. These findings support a bichromophoric character for our ruthenium complexes in the ground state, a necessary condition in the design of supramolecular systems for the study of electron transfer. Photophysical studies indicate fast quenching of the triplet excited state in both complexes, which suggests strong intercomponent excited-state interactions. Evidence is presented that this quenching is due to intramolecular electron transfer, at least in the case of $[Ru(bpy)_2(DPSalH_2)]^{2+}$, for which a charge-separated state with a remarkable lifetime of about 30 μs was observed.

Keywords: copper · electron transfer · ligand design · photochemistry · ruthenium

Introduction

Research in the field of photoinduced energy and electron transfer using supramolecular model compounds is fueled by the increasing interest of chemists in charge-separation devices,[1] light-harvesting species,[2] optoelectronics[3] and photocatalysts.[4] The basic architecture of such supramolecular systems for the study of electron and energy transfer comprises two covalently tethered components. Extensive studies on photoinduced electron transfer have been realised in Ru^{II}–Os^{III} dinuclear complexes. In these systems, the Ru^{II} polypyridine metal complex plays the role of photosensitiser, whereby its lowest excited state is responsible for driving the electron transfer process, while the Os^{III} complex acts as an internal electron acceptor.[5] Electron transfer is mediated through a bridging ligand which thus plays an essential role in the proper functioning of these systems. Primarily, it sets the distance and spatial orientation of the two fundamental constituents, that is, the donor and acceptor parts. It controls the electronic communication between the two chromophores and therefore the rate of electron transfer.[6] Hence, the inaugural step in this research area is the design and construction of the molecular spacer that will

[a] Dr. Y. Pellegrin, Dr. P. Dorlet, Dr. M. F. Charlot, Prof. A. Aukauloo
Laboratoire de Chimie Inorganique, UMR 8613
Université de Paris-Sud, 91405 Orsay (France)
E-mail: aukauloo@icmo.u-psud.fr

[b] Dr. A. Quaranta, Dr. W. Leibl
Service de Bioénergétique, CEA Saclay
Bât. 532, 91191 Gif-sur-Yvette Cedex (France)
E-mail: leibl@dsvidf.cea.fr

[c] Dr. A. Quaranta
Muséum National d'Histoire Naturelle
Laboratoire de Chimie et de Biochimie des Substances Naturelles
UMR 5154 CNRS/USM 0502 CNRS, 63 rue Buffon 75005 Paris (France)

Supporting information for this article is available on the WWW under http://www.chemeurj.org/ or from the author.

DOI: 10.1002/chem.200401064

hold the two partners, each with well-defined properties. A plethora of bridging ligands containing identical anchoring sites has been developed for this purpose.[7]

More recently, the idea of using $[Ru(bpy)_3]^{2+}$ as photosensitiser to develop new photocatalysts emerged. An archetypal system is a $[Ru(bpy)_3]^{2+}$ complex covalently linked to a transition metal complex which can be reduced (or oxidised) following a reductive (oxidative) quenching pathway of the ^{3}MLCT state of the photosensitiser.[8] Electron transfer in these supramolecular systems is realised in a similar fashion as in noncovalently attached bimolecular systems, that is, by addition of exogenous electron donors or acceptors.[9] As mentioned above, the nature and structure of the bridging ligand is of primary importance in this field. Moreover, heteroditopic ligands, that is, bearing two different coordinating sites, developed to accomodate both metal ions, have a bipyridine moiety to bind to the photosensitiser and a polydentate core for the transition metal ion. Along this line, we recently reported on a rigid heteroditopic ligand containing a dipyrridophenazine moiety and a salophenic cavity.[10]

In our continuing effort to develop bridging ligands to attach an Ru^{II} polypyridine and a first-row transition element, we report here the synthesis of the novel heteroditopic ligand *N*,*N*′-bis(3,5-di-*tert*-butylsalicylidene)-5,6-(1,10-phenanthroline)diamine (abbreviated $DPSalH_2$ as a shorthand for *dip*yrrido-*N*,*N*′-bis(3,5-di-*tert*-butyl*sal*icylidene)-1,2-phenylenediamine) that can be regarded as a fusion of phenanthroline and a tetradentate Schiff base cavity. In comparison with our previous work, the phenazine moiety is missing, and hence the distance and the electronic communication between the metal ions are expected to be altered. In a stepwise manner, attachment of the diimine end of $DPSalH_2$ to ruthenium to give $[Ru(bpy)_2(DPSalH_2)]^{2+}$ was followed by metallation of the salophenic cavity with copper(II) to give $[Ru(bpy)_2(DPSalCu)]^{2+}$. The electronic influence of the Ru^{II} ion on the N_2O_2 cavity of $DPSalH_2$ and on the Cu^{II} complex in $[Ru(bpy)_2(DPSalCu)]^{2+}$ and vice versa were evaluated by comparing the physicochemical properties of $SalH_2$ and SalCu (where $SalH_2$ is the proligand and stands for *N*,*N*′-bis(3,5-di-*tert*-butylsalicylidene)-1,2-phenylenediamine).
Density functional calculations were performed on $DPSalH_2$, DPSalCu and $[Ru(bpy)_2(DPSalH_2)]^{2+}$ derivatives, and our theoretical data corroborate our electrochemical studies. Photophysical studies showed fast quenching of the ^{3}MLCT state for both complexes, resulting in a long-lived intramolecular charge-separated state in the case of $[Ru(bpy)_2(DPSalH_2)]^{2+}$, but not in the case of $[Ru(bpy)_2(DPSalCu)]^{2+}$.

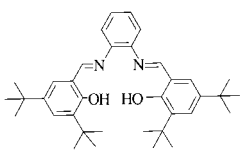

$SalH_2$

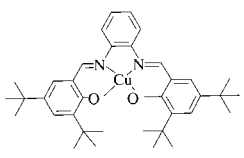

SalCu

Results and Discussion

Synthesis: Ligand $DPSalH_2$ was prepared in a straightforward manner by condensation of two equivalents of 3,5-di-*tert*-butylsalicylaldehyde with 1,10-phenanthroline-5,6-diamine in boiling ethanol in the presence of triethyl orthoformate. In the absence of triethyl orthoformate, a mixture of mono- and dicondensed products was isolated, probably due to the less basic character of the amino groups on the phenanthroline moiety. Thus, triethyl orthoformate must drive the reaction to completion by eliminating water molecules of condensation. The binding of the bipyridine cavity of $DPSalH_2$ to $[Ru(bpy)_2]^{2+}$ was carried out in MeOH, followed by insertion of copper(II) into the salophen coordinating site according to literature procedures[11] (Scheme 1) and

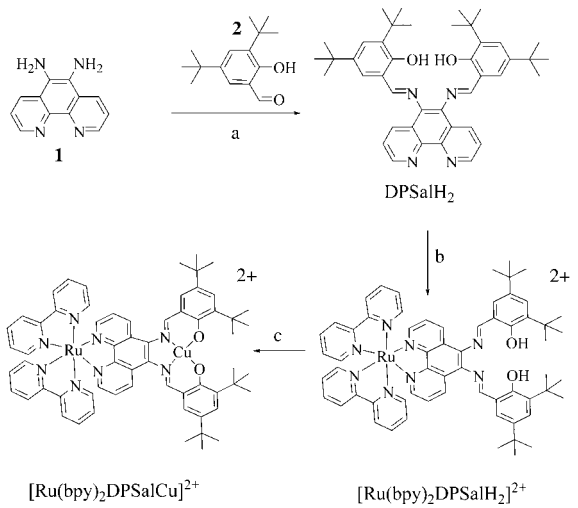

Scheme 1. Synthetic pathway. a) Reflux in $EtOH/HC(OEt)_3$; b) reflux with $[Ru(bpy)_2](NO_3)_2$ in $CH_2Cl_2/HC(OEt)_3$; c) stir with $Cu(OAc)_2$ in MeOH at RT.

the compounds were isolated as the perchlorate salts. Prior to photophysical and spectroelectrochemical studies $[Ru(bpy)_2(DPSalH_2)]^{2+}$ and $[Ru(bpy)_2(DPSalCu)]^{2+}$ were purified by chromatography on neutral alumina with dichloromethane/methanol (95/5 and 90/10, respectively) as eluent and were recovered as the first fractions.

^{1}H NMR spectra: All the expected NMR features were identified for $DPSalH_2$ and $[Ru(bpy)_2(DPSalH_2)]^{2+}$. Figure 1 shows the aromatic part of the ^{1}NMR spectra of the ligand and its ruthenium complex. All signals were assigned after 2D ^{1}H NMR experiments. Of particular interest is the observed shift of the iminic protons on metallation with ruthenium(II).

IR spectroscopy: IR spectra were diagnostic of the metallation step of $DPSalH_2$. Docking of the phenanthroline end of $DPSalH_2$ to ruthenium was revealed by the CH vibrations of the *tert*-butyl groups at around 2950 cm^{-1} together with

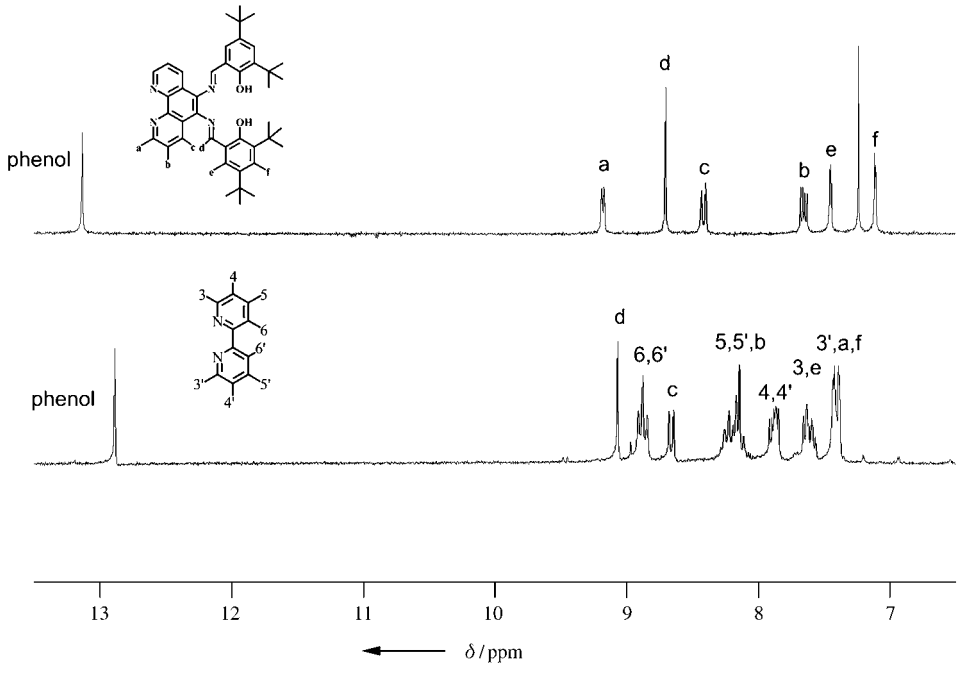

Figure 1. ^{1}H NMR spectra of $DPSalH_2$ in $CDCl_3$ and $[Ru(bpy)_2(DPSalH_2)](ClO_4)_2$ in [D$_6$]DMSO.

the intense symmetric and antisymmetric stretching of the imine groups at 1615 and 1585 cm^{-1}, respectively. No apparent shift was observed for the imine absorption bands of mononuclear complex $[Ru(bpy)_2(DPSalH_2)](ClO_4)_2$, but a marked red shift of about 50 cm^{-1} occurred when copper(II) was present in the salophenic cavity. A shift of only 20 cm^{-1} was observed for the same bands on going from the $SalH_2$ ligand to the corresponding copper(II) complex.[12] This difference can be tentatively attributed to a structural rearrangement of the N_2O_2 cavity on insertion of Cu^{II}, whereby the C=N bonds would feel the presence of both divalent ions. A distortion of the tetracoordinating cavity due to the iminic hydrogen atoms (d) and hydrogen atoms at the c-positions on the phenanthroline moiety may also account partly for this low-energy shift of these vibrations.

Electrospray mass spectrometry: ESI-MS spectra of the ruthenium complexes consolidate the different structures reported herein. The mass spectrum of $[Ru(bpy)_2(DPSalCu)](ClO_4)_2$ shows a parent peak at 558.7 corresponding to the dicationic species. The experimental and simulated spectra are shown in Figure 2.

UV/Vis spectroscopy: Electronic absorption data are summarised in Table 1; data for $SalH_2$ and SalCu are also included. The free ligand $DPSalH_2$ is characterised by two intense absorption bands corresponding to intraligand π–π* transitions at 280 and 350 nm. The electronic spectrum of $[Ru(bpy)_2(DPSalH_2)]^{2+}$ shows characteristic features of $[Ru(bpy)_3]^{2+}$, that is, strong π–π* transitions for the bipyridine moieties at 290 nm and a characteristic MLCT band in the range 400–500 nm tailing up to 560 nm, together with a band at around 350 nm illustrating the presence of coordinated $DPSalH_2$. It is noteworthy that no change in energy and intensity is noticed for the MLCT (d_π–π* bpy) band when compared to $[Ru(bpy)_3]^{2+}$, which argues that no electronic change is perceptible by the ruthenium(II) ion and hence supports a bichromophoric character for $[Ru(bpy)_2(DPSalH_2)]^{2+}$ (Figure 3).[13]

However, subtle spectral modifications are observed on insertion of copper(II) into the salophenic cavity. For comparison, the absorption spectrum of an equimolar mixture of $[Ru(bpy)_3]^{2+}$ and SalCu is also presented (Figure 3). Clearly, the electronic spectrum of $[Ru(bpy)_2(DPSalCu)]^{2+}$ is not a mere algebraic sum of those of $[Ru(bpy)_3]^{2+}$ and SalCu. The π–π* transitions of the bipyridine in the high-energy region (290 nm) remain unchanged on insertion of Cu^{II} into the tet-

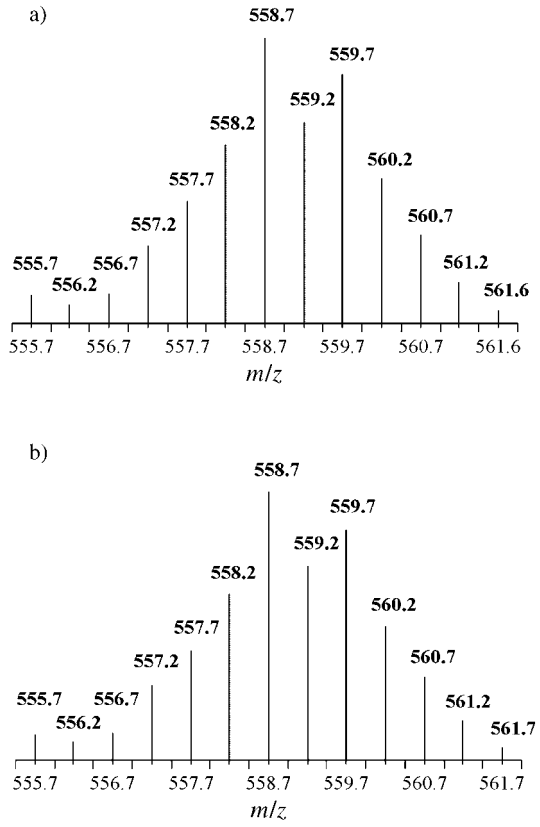

Figure 2. Experimental (a) and simulated (b) ESI-MS spectra of $[Ru(bpy)_2(DPSalCu)](ClO_4)_2$.

Table 1. UV/Vis data.

	λ [nm] (ε [10^{-3} L mol^{-1} cm^{-1}])
$DPSalH_2$[a]	355 (1.62), 280 (4.78)
$[Ru(bpy)_2(DPSalH_2)]^{2+}$[b]	452 (1.99), 425 (sh), 355 (sh), 285 (9.29)
$[Ru(bpy)_2(DPSalCu)]^{2+}$[b]	480 (3.31), 455 (3.04), 378 (2.57), 325 (3.99), 285.3 (7.93)
$SalH_2$[a]	340 (1.74), 281 (2.51)
SalCu[b]	446 (1.99), 405 (sh), 348 (sh), 331 (2.50), 315 (2.83), 302 (sh), 250 (3.55)

[a] In dichloromethane. [b] In acetonitrile.

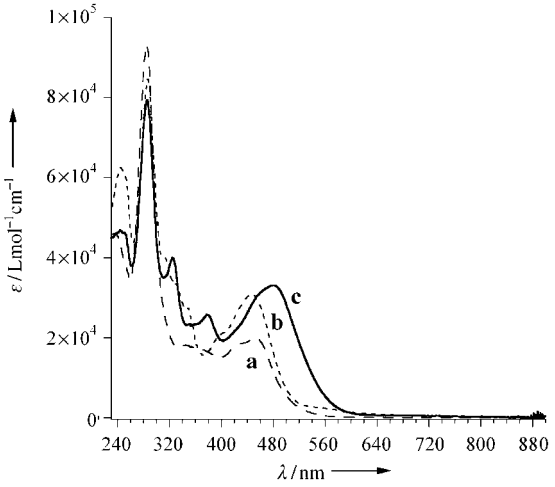

Figure 3. Absorption spectra in MeCN: a) $[Ru(bpy)_2(DPSalH_2)]^{2+}$, b) equimolar mixture of $[Ru(bpy)_3]^{2+}$ and SalCu, and c) $[Ru(bpy)_2(DPSalCu)]^{2+}$.

racoordinating cavity. Two bands at 325 and 380 nm are attributed to charge-transfer transitions within the $DPSalCu^{II}$ component, as such transitions are observed for SalCu between 315 and 350 nm. The shift to lower energies of these bands may be due to the more delocalised π system of the phenanthroline. However, the main feature is the broad unsymmetrical band extending from 400 to 580 nm, which probably contains contribution of charge-transfer transitions from both components. The bathochromic shift and the increase in intensity of this band compared to that of the equimolar mixture of $[Ru(bpy)_3]^{2+}$ and SalCu may indicate some electronic communication between the covalently linked partners.

EPR study of $[Ru(bpy)_2(DPSalCu)]^{2+}$: The EPR spectra of $[Ru(bpy)_2(DPSalCu)]^{2+}$ and SalCu, recorded at 100 K in ethanol/methanol (4/1), are shown in Figure 4. They exhibit an axial powder pattern with superhyperfine structure in the perpendicular region. These superhyperfine interactions arise from the two coordinated nitrogen nuclei ($I=1$) and the iminic protons ($I=1/2$).[14] Simulations were performed to extract the g and hyperfine parameters for the copper ion in both complexes (Table 2). The simulations also included superhyperfine parameters for the four hydrogen and nitrogen nuclei to account for the structure observed in the spectra. However, only an estimate of these parameters could be

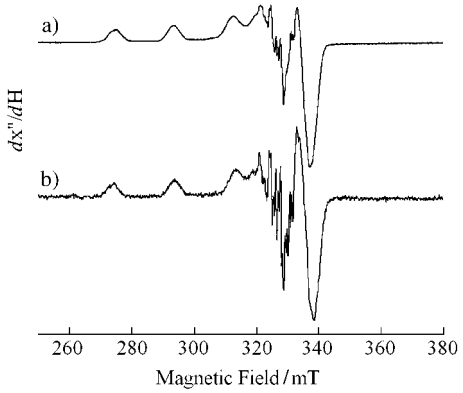

Figure 4. EPR spectra of a) $[Ru(bpy)_2(DPSalCu)]^{2+}$ and b) SalCu at 100 K in EtOH/MeOH (4/1). Experimental conditions: a) $T=120$ K, $\nu_{mw}=9.38338$ GHz, amplitude modulation 0.2 mT, microwave power 16 mW, modulation frequency 100 kHz, 4 scans; b) $T=100$ K, $\nu_{mw}=9.37698$ GHz, amplitude modulation 0.1 mT, microwave power 0.5 mW, modulation frequency 100 kHz, 4 scans.

Table 2. EPR parameters obtained from simulations of the spectra.

	$[Ru(bpy)_2(DPSalCu)]^{2+}$	SalCu
$g_\parallel$	2.213	2.206
$g_\perp$	2.046	2.046
$10^4 A_\parallel$ [cm^{-1}]	191.8	200.1
$10^4 A_\perp$ [cm^{-1}]	21.1	25.2
$g_\parallel/A_\parallel$ [cm]	115	110

obtained due to the difficulty in reproducing exactly the features observed experimentally. ENDOR experiments are underway to determine more accurately the superhyperfine couplings. Preliminary ENDOR data for $[Ru(bpy)_2(DPSalCu)]^{2+}$ show that the nitrogen hyperfine interaction is mainly isotropic with a value of 38 MHz, which is in agreement with values reported for similar complexes.[15]

Comparison between the parameters of the copper ions for the two complexes shows an increase in $g_\parallel$ and a decrease in $A_\parallel$ for the dinuclear complex compared to SalCu. This is an indication of a distortion of the copper site for the ruthenium-containing complex compared to square-planar SalCu. This distortion introduces some mixing of the d_{z^2} orbital into the $d_{x^2-y^2}$ orbital occupied by the unpaired electron, which leads to less spin density on the copper ion and therefore to a decrease in the hyperfine interaction. However, this distortion is expected to be small, as reflected by the close values of the empirical distortion parameter $g_\parallel/A_\parallel$ calculated for the two complexes (Table 2).[16]

Electrochemical behaviour: Redox behaviour of covalently linked multicomponent systems often reflects the electronic coupling between the constituent units.[17] Three different cases can be expected: 1) a strong interaction resulting in a different redox behaviour of the assembled units, 2) a weak interaction leading to slight modification of the electron-transfer processes and 3) negligible coupling and hence juxtaposition of redox properties for each subunit. Usually, to rationalise the redox properties of these supramolecular spe-

cies, it is important to take into account the electrochemical behaviour of each subunit. Hence, for this study we also recorded the cyclic voltammograms (CV) of $SalH_2$ and the corresponding copper complex SalCu under similar experimental conditions. All redox data are collected in Table 3.

Table 3. Potentials E from cyclic voltammetry at 100 mV s^{-1} for oxidations (i, ii) and reductions (I, II, III) for $DPSalH_2$, $[Ru(bpy)_2(DPSalH_2)]^{2+}$, $[Ru(bpy)_2(DPSalCu)]^{2+}$, $SalH_2$ and SalCu.

	^{III}E	^{II}E	^{I}E	^{i}E	^{ii}E
$DPSalH_2$[a]				+1.24[b]	+1.51[b]
$[Ru(bpy)_2(DPSalH_2)]^{2+}$[c]	−1.59[d]	−1.39[d]	−1.17[c]	+1.28[b]	+1.37[b]
$[Ru(bpy)_2(DPSalCu)]^{2+}$[c]	−1.61[d]	−1.39[d]	−0.81[d]	+0.90[d]	+1.43[b]
$SalH_2$[a]				+1.20[b]	+1.60[b]
SalCu[c]			−1.30[d]	+0.94[d]	+1.14[c]

[a] Measured in dichloromethane. [b] Irreversible step, anodic peak given. [c] Measured in acetonitrile. [d] $E_{1/2}=1/2(E_{pa}+E_{pc})$ in V versus SCE in presence of 0.1 M $TBAClO_4$. [e] Irreversible step, cathodic peak given.

$SalH_2$, $DPSalH_2$ and $[Ru(bpy)_2(DPSalH_2)]^{2+}$: The CV of $DPSalH_2$ in MeCN (Figure 5a) shows no reduction wave within the scanned potential window (−2 V versus SCE) and two nonreversible oxidation waves at quite high potentials which are assigned to the oxidation of the phenol groups. Such a redox behaviour is closely related to that of $SalH_2$, which shows a similar CV under the same experimental conditions. The electrochemical behaviour of $[Ru(bpy)_2(DPSalH_2)]^{2+}$ conforms to that of a $[Ru(bpy)_3]^{2+}$-type complex (Figure 5) and, as expected for a heteroleptic complex, the reduction pattern gives a clear indication of the energy levels of the π* orbitals of the ligands in the coordination sphere of Ru^{II}.[10,18] Three reduction waves are observed while scanning down to −2 V versus SCE, the first of which (ca. −1.17 V) is nonreversible in nature, whereas the second and third waves (−1.40 and −1.60 V) are reversible processes. The main difference between the CVs of $[Ru(bpy)_2(DPSalH_2)]^{2+}$ and $[Ru(bpy)_3]^{2+}$ is the irreversible character and the shift to more positive potential of the first reduction wave. This implies the presence of $DPSalH_2$ in the coordination sphere of ruthenium and that the addition of the first electron more likely occurs on the coordinated $DPSalH_2$ due to its more electron accepting character than bpy because of the two imino groups. The irreversible character of this wave under our experimental conditions suggests that the addition of one electron on the imine moiety is followed by a chemical reaction, probably a proton transfer from the nearby phenolic OH group. On the anodic side of the CV, oxidative peaks for the phenol group together with that of Ru^{II} appear almost at the same potential. A differential pulsed cyclic voltammogram allowed us to separate the different redox waves, and the first is assigned to the oxidation of the phenol group, while the potential for the Ru^{III}/Ru^{II} (+1.37 V versus SCE) falls within the typical potential range for $[Ru(diimine)_3]^{2+}$ complexes.

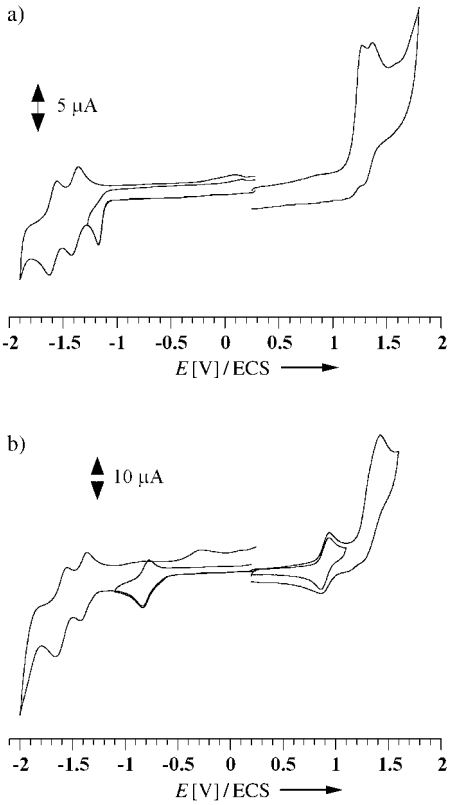

Figure 5. Cyclic voltammograms in MeCN (10^{-3} M solutions, room temperature, sweep rate 100 mV s^{-1}, $Ag/AgClO_4$ electrode as reference, 0.1 M $TBAClO_4$ as supporting electrolyte). a) $[Ru(bpy)_2(DPSalH_2)]^{2+}$ and b) $[Ru(bpy)_2(DPSalCu)]^{2+}$.

SalCu and $[Ru(bpy)_2(DPSalCu)]^{2+}$: The CV of SalCu (see Supporting Information) in dichloromethane shows one reversible reduction wave (−1.30 V versus SCE), ascribed to the reduction of Cu^{II} to Cu^{I}, and two reversible oxidation peaks (+0.94 and +1.14 V versus SCE, respectively) corresponding to the sequential oxidation of the deprotonated phenol groups. The locus of oxidation was assigned after spectroelectrochemical studies and furthermore confirmed by a recent paper of Pratt et al.[19] Indeed, the UV/Vis/NIR spectrum of the monooxidised species shows absorption bands in the NIR (800–1500 nm) region that are characteristic of a bound phenoxyl radical.[20]

Upon reduction, $[Ru(bpy)_2(DPSalCu)]^{2+}$ is characterised by three reversible redox processes at −0.81, −1.39 and −1.60 V versus SCE (Figure 5b). This sequence of steps can be compared with that of $[Ru(bpy)_2(DPSalH_2)]^{2+}$, where the main difference is the positive shift of the first reduction wave. The second and third reductions occur at almost the same potentials in both cases and are in favour of sequential addition of one electron to the two unmodified bipyridine ligands. However, the positive shift of 360 mV for the first reduction wave is quite remarkable. Two proposals can account for this wave: a ligand- or a metal-centred (Cu^{II}/Cu^{I}) reduction. In the case of a ligand-centred process, it implies that the presence of the copper(II) ion in the salophenic

cavity facilitates uptake of the first electron by the ditopic ligand skeleton. On the other hand, if electron addition involves the copper(II) center, this would imply a positive shift of about 500 mV (from SalCu to $[Ru(bpy)_2(DPSalCu)]^{2+}$) based only on a Coulombic effect.[21] Spectroelectrochemical studies on the addition of the first electron showed only minor modification of optical properties. The EPR spectrum of the electrolysed solution always shows the presence of unreduced material caracterised by copper(II) signals, and this prevents a more detailed spectroscopic analysis.

Two main features are observed on the anodic side of the cyclic voltammogram of $[Ru(bpy)_2(DPSalCu)]^{2+}$, that is, a reversible one-electron process at $+0.90$ V and a second nonreversible wave which includes the oxidation of Ru^{II} at $+1.37$ V versus SCE. The UV/Vis/NIR signature of the species following abstraction of the first electron was monitored at room temperature in an optically transparent thin-layer cell in the presence of 0.1 M $TBAClO_4$ at $+1.0$ V (Figure 6).

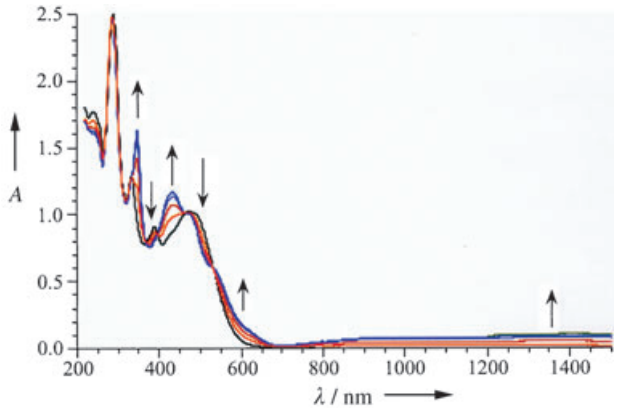

Figure 6. Electronic absorption spectra on electrolysis at controlled potential in MeCN (10^{-3} M solutions, room temperature, SCE as reference, 0.1 M $TBAClO_4$ as supporting electrolyte). For $[Ru(bpy)_2(DPSalCu)]^{2+}$ on oxidation at $+1.0$ V/SCE. A = absorbance.

Chemical reversibility of this electron-transfer process was evidenced by total recovery of the initial spectrum on reduction, and the presence of several isosbestic points clearly indicates that only two species are in equilibrium in solution. The main changes in the optical spectrum on abstraction of the first electron can be closely related to the spectral modification on oxidation of SalCu to $[SalCu]^+$ (see Supporting Information). Broad bands in the NIR region (800–1500 nm) and alteration of the charge-transfer bands in the visible region are generally observed for the generation of a metalloradical species. It is noteworthy that the π–π* transition for the bpy moiety at 290 nm is almost unaltered, which reaffirms that this process is decoupled from the bpy moiety. However, attribution of spectral change in the region 450–600 nm is precluded as it probably involves CT transitions of both components. An important experimental observation is the negligible potential shift for the first oxidation wave between $[Ru(bpy)_2(DPSalCu)]^{2+}$ and SalCu. Furthermore, spectroscopic data for the singly oxidised species of $[Ru(bpy)_2(DPSalCu)]^{2+}$ clearly indicates that the locus of oxidation is unaltered in the dinuclear complex. Likewise, the oxidation potential for the Ru^{III}/Ru^{II} couple seems unaffected when Cu^{II} is present in the N_2O_2 cavity, that is, no Coulombic effect is experienced. These observations support the idea that the electronic properties of each component are maintained in the covalently attached system, which hence can be classified as a supramolecular assembly. If we follow the same argument, then it is unlikely that such a Coulombic effect is operative for the first electron on reduction. Hence, a ligand-centred reduction is favoured for the first reduction process, whereby the presence of two divalent ions should enhance the stability for electron uptake by the organic skeleton holding the two metal centers.

Theoretical calculations: DFT calculations were employed to assess the energy levels and the electronic maps of the LUMO and HOMO of the free ligand and its corresponding copper complex. The computed data are necessary to shed light on the electrochemical properties and the absorption spectra of the ruthenium complexes. The geometries of the studied species were optimised at the B3LYP/LanL2DZ level. To shorten these lengthy calculations we omitted the *tert*-butyl groups on the phenol rings and retained C_2 symmetry for calculations on $DPSalH_2$ and DPSalCu. Test computations on the free ligand with four *t*Bu groups or with C_1 symmetry showed that the nature and energy order of the frontier orbitals are only slightly affected. Our computed metric data are in good agreement with experimentally available values, though, as usual, the calculated values are somewhat higher than the observed ones.[22] Steric congestion between the protons of the phenanthroline end and the iminic protons (c and d, respectively, see Figure 1) leads to a departure from coplanarity of the phenanthroline skeleton and the salophenic cavity. The main torsion occurs around the C(phen)–N(imine) bond. For $DPSalH_2$, N(imine)···H-(phenol) hydrogen bonds stabilize several conformations (in our gas-phase calculations) but no planar tetracoordinating N_2O_2 cavity mode was found. For DPSalCu, the computed geometry of the copper ion is slightly distorted square-planar, in agreement with the EPR data.

Figure 7 shows the frontier orbitals for $DPSalH_2$ with the corresponding energy levels and symmetry labels in C_2 symmetry. As our interest is in the ditopic nature of the ligand, similar calculations were performed on the phenanthroline and $SalH_2$ building blocks with C_{2v} and C_2 symmetry, respectively (Figure 7). The frontier MOs of the free ligand can be classified as being more predominantly developed on the phenanthroline end ("phen-like") or on the salophenic skeleton. The two lowest vacant molecular orbitals consist essentially of the a and b combinations of the antibonding π* orbitals of the imino (C=N) groups with small contributions on the phenol groups and almost no contribution on the phenanthroline extremity. In contrast, the LUMO+2 (b) and LUMO+3 (a) are more phen-like. Interestingly, the energies and electronic distributions of these two orbitals are similar to those of the LUMO+1 (b_1 ψ) and LUMO (a_2 χ)

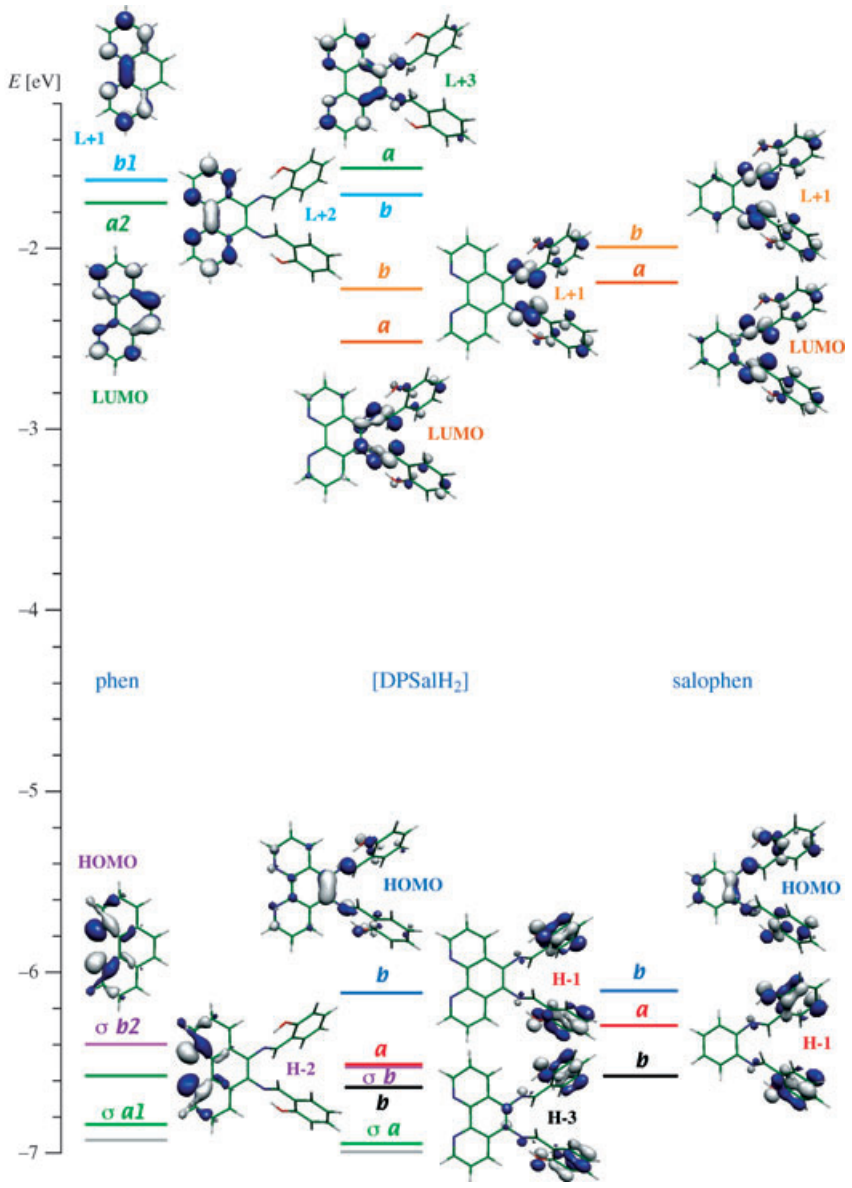

Figure 7. Frontier orbitals for phenanthroline, $SalH_2$ and $DPSalH_2$ (*t*Bu groups replaced by H for simplification).

of phenanthroline, respectively. As ψ and χ invert their order going from bpy to phen, the LUMO+2 of the ligand is almost the LUMO of bpy. In contrast to the localised character of the LUMOs, for the HOMO the electron density distribution is located both on the bipyridine end and, to a larger extent, on the ancillary Schiff base. The HOMO−1 and HOMO−2 (almost degenerate) are the combination of phenol MOs and the b_2 (σ-type) orbital of phen, respectively.

Because of the paramagnetic nature of DPSalCu, spin-unrestricted calculations were performed. Corresponding pairs of α and β spin orbitals have, as expected, nearly the same energy and spatial extent (constituting an MO) except for the $d_{x^2-y^2}$-type copper-centred spin orbitals, occupied for α spin (unpaired electron) and vacant for β spin. An orbital scheme is shown in Figure 8. The highest occupied and lowest unoccupied orbitals both extend essentially over the salophenic chromophore. The LUMO has a small contribution on phen, but not on the nitrogen atoms susceptible to coordinate to ruthenium. Its electronic distribution is reminiscent of the LUMO of the free ligand but, as a consequence of coordination to copper, the antibonding π* character of the imino groups is strongly decreased. The LUMO in DPSalCu is hence stabilised as compared to $DPSalH_2$. The HOMO of DPSalCu differs from the HOMO of the free ligand as it has a slight metallic character and an important contribution of the phenol groups, especially the coordinating oxygen atoms.

The theoretical data obtained for $DPSalH_2$ and DPSalCu were used to substantiate the electrochemical behaviour of our complexes. However, data calculated for the free ligand and copper compound must be considered with caution when extrapolated to the properties of the ruthenium complexes.

Considering first $[Ru(bpy)_2(DPSalH_2)]^{2+}$, the fact that the two lowest vacant MOs of the free ligand are localised on the salophenic skeleton with no electronic contribution on the phenanthroline, especially on the nitrogen atoms, suggests that no orbital mixing will occur with the d_π orbitals of the ruthenium center. We can tentatively assume that there is no drastic energy change for these MOs on coordination with Ru^{II}. In contrast, the LUMO+2 will mix approximately in the same way as the LUMO of bpy. This can explain why no bathochromic shift is observed for the MLCT d_π–πbpy transition in the absorption spectrum of the ruthenium complex in comparison with the $[Ru(bpy)_3]^{2+}$ chromophore, despite the lower energies of the first two LUMOs of the ditopic ligand. Turning to electrochemical properties and assuming that the calculated LUMO must be the locus for uptake of the first electron, the preceding remarks allow us to conclude that the first electron must be localised on $DPSalH_2$ and more precisely

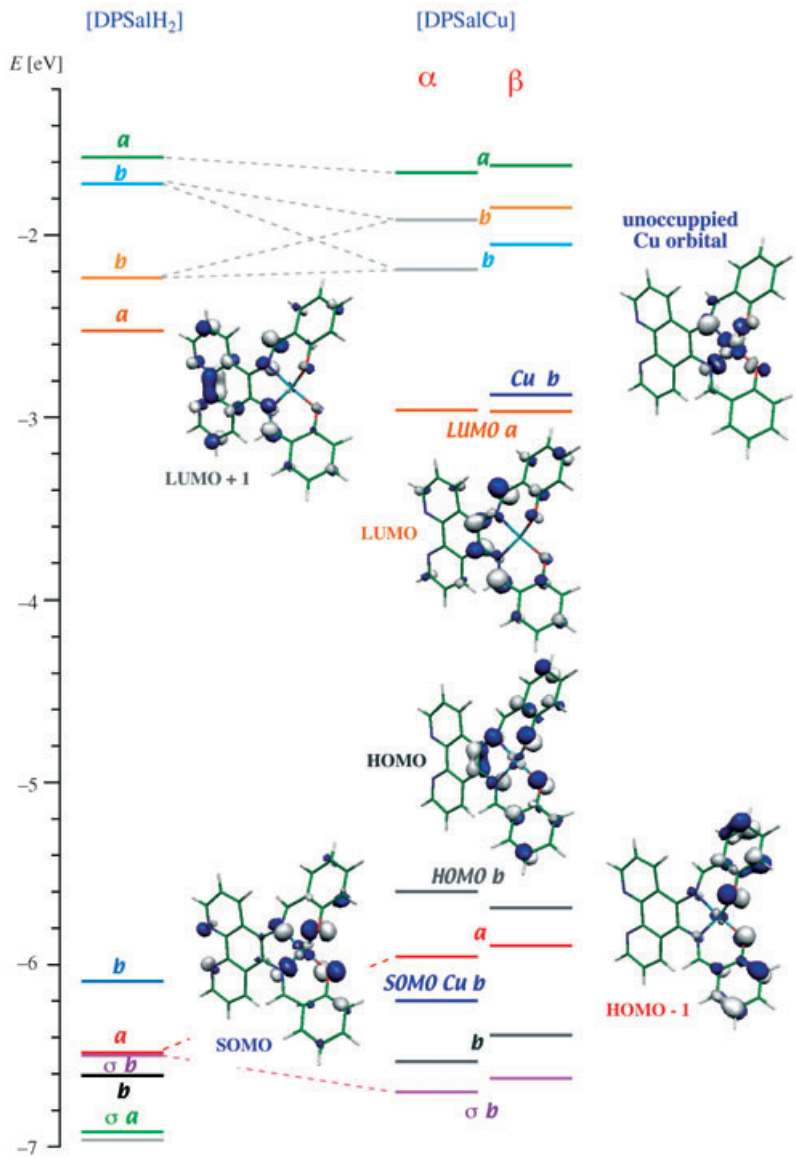

Figure 8. MO correlation between $DPSalH_2$ and DPSalCu.

on the strong π-electron acceptor imino groups. This agrees with the conclusions from the electrochemical behaviour.

On metallation with Ru^{II}, orbital HOMO−2, which is responsible for the Ru–ligand σ bond, will be strongly lowered in energy; one can also expect a small stabilisation of the HOMO by π interaction of the bpy end of the ligand with ruthenium. Preliminary calculations on $[Ru(bpy)_2(DPSalH_2)]^{2+}$ were performed in C_2 symmetry by using the calculated structure of $DPSalH_2$ together with that of $[Ru(bpy)_3]^{2+}$. Both the distances of the metal-coordinating nitrogen atoms and the angles around Ru^{II} were optimised. As indicated in Figure 9, the computed HOMO for $[Ru(bpy)_2(DPSalH_2)]^{2+}$ is mainly distributed on the phenol rings with a small contribution on the imino nitrogen atoms. As can be visualised, this HOMO of b symmetry is similar to HOMO-3 of the free ligand.

Similarly, the electrochemical behaviour of $[Ru(bpy)_2(DPSalCu)]^{2+}$ can be analysed. The calculated LUMO for DPSalCu clearly indicates the nonparticipation of the coordinating nitrogen atoms of the bipyridine, and hence it is most probable that this MO is only slightly altered both energetically and electronically in the dinuclear complex. In fact, as pointed out in the electrochemical studies, the first reduction process indeed implies the addition of one electron on the heteroditopic ligand and not on the bpy or the copper ion. The positive shift noticed for this electron-transfer process as compared to the mononuclear ruthenium complex can be interpreted by stabilisation of the ligand-centred LUMO in the presence of copper. The first oxidation process is also confirmed as being a removal of one electron from a ligand-centered (essentially on phenol groups) molecular orbital with generation of a metalloradical. Preliminary computed data for the one-electron-deficient species $[DPSalCu]^+$ are in favour of an MO mostly localised on the phenol rings.

Photophysical measurements: Measurements of luminescence lifetime, triplet transient absorption and electron transfer were carried out to investigate the effect of the $DPSalH_2$ ligand and of copper in the salophenic cavity on the fate of

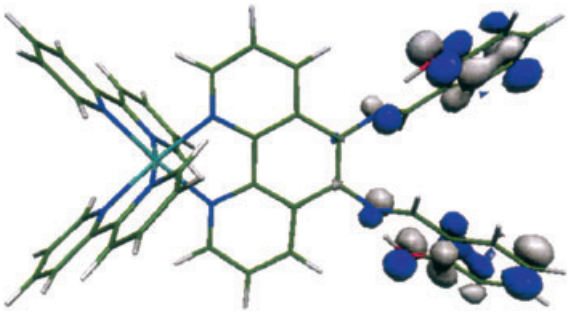

Figure 9. HOMO of $[Ru(bpy)_2(DPSalH_2)]^{2+}$ (*t*Bu groups replaced by H for simpliflication).

the excited state of the lumophore. In Ru polypyridine complexes, intersystem crossing from the singlet excited state to the triplet excited state occurs within few hundred femtoseconds[23] and thus all photochemistry initiates from the lowest triplet excited state.

From time-resolved picosecond luminescence measurements, the emission lifetime of the complexes in ethanol was determined. As shown in Figure 10, the emission yield is

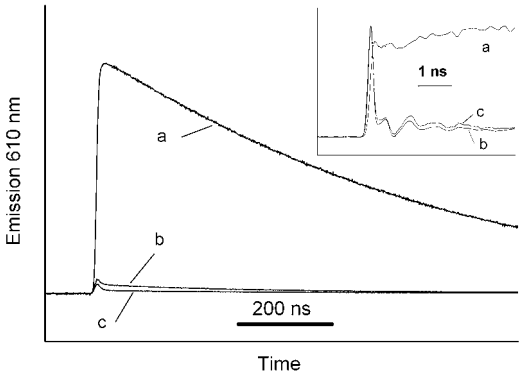

Figure 10. Emission kinetics at 610 nm on excitation with a nanosecond laser flash (532 nm). a) $Ru(bpy)_3^{2+}$, b) $[Ru(bpy)_2(DPSalH_2)](ClO_4)_2$ and c) $[Ru(bpy)_2(DPSalCu)](ClO_4)_2$ in argon-saturated EtOH. Sample concentrations were adjusted for equal absorption at the excitation wavelength. Inset: emission kinetics at 610 nm on excitation with a picosecond laser flash (532 nm) and traces normalised to equal maximum amplitude.

strongly reduced in both complexes as compared to the parent lumophore. The luminescence of $[Ru(bpy)_2(DPSalH_2)]^{2+}$ and $[Ru(bpy)_2(DPSalCu)]^{2+}$ in argon-saturated ethanol at 610 nm is characterised by a biexponential decay consisting of a dominant fast phase which is not time-resolved in these experiments and a slow component ($\tau \approx 800$ ns). The fast phase, the relative amplitude of which is slightly larger for $[Ru(bpy)_2(DPSalCu)]^{2+}$ than for $[Ru(bpy)_2(DPSalH_2)]^{2+}$, is absent in $[Ru(bpy)_3]^{2+}$. Emission measurements with higher time resolution on a faster time scale (Figure 10, inset) confirmed that the fast decay is characterised by a lifetime of $\tau < 100$ ps. Comparison of the emission characteristics of $[Ru(bpy)_3]^{2+}$ and $[Ru(bpy)_2(DPSalH_2)]^{2+}$ suggests that the observed quenching of emission is related to the presence of the ligand and is likely to be due to intramolecular electron transfer. The presence of Cu^{II} in the salophenic cavity of the ligand enhances the quenching process, which could be due to faster intramolecular electron transfer or fast energy quenching by the Cu^{II} ion followed by radiationless decay. The small decay phase present in both complexes with low relative amplitude (a few percent of the overall decay) exhibits kinetics very similar to those of $[Ru(bpy)_3]^{2+}$. As no trace of $[Ru(bpy)_3]^{2+}$ could be detected in $[Ru(bpy)_2(DPSalH_2)]^{2+}$ and $[Ru(bpy)_2(DPSalCu)]^{2+}$ by mass spectroscopy, its origin in our complexes is still unclear.

To characterise the reaction product formed after decay of the excited state, flash-induced absorption difference spectra were recorded in the visible and near-infrared spectral range. Figure 11 shows the transient absorption spectra of our mono- and dinuclear complexes. Whereas $[Ru(bpy)_2(DPSalH_2)]^{2+}$ displays large absorption changes throughout this spectral range, only very weak changes were detected in the case of the Ru/Cu complex. Common features can be distinguished in the spectra of $[Ru(bpy)_3]^{2+}$ and $[Ru(bpy)_2(DPSalH_2)]^{2+}$. Both exhibit bleaching of the ground-state absorption centred around 450 nm and the appearance of a very broad absorption band for wavelengths greater than 500 nm and extending into the near infrared. On the other hand there are differences in relative amplitudes of absorption bands and the lifetime of the flash-induced absorption changes. While for $[Ru(bpy)_3]^{2+}$ the relative amplitude of the bleaching at 450 nm is much larger than the amplitude of the absorption increase in the red region, it is similar for $[Ru(bpy)_2(DPSalH_2)]^{2+}$. Concerning the kinetics, the decay of the absorption changes in the latter (about 30 μs) is much slower than in $[Ru(bpy)_3]^{2+}$, for which the absorption change disappears with the same kinetics as the luminescence (800 ns). This shows that the observed absorption changes for $[Ru(bpy)_2(DPSalH_2)]^{2+}$ are not related to the MLCT state, as is the case for $[Ru(bpy)_3]^{2+}$. In agreement with earlier studies on similar Ru complexes,[10] the broad absorption band in the red region is attributed to an organic radical species generated by intramolecular electron transfer to form the state $[Ru^{III}(bpy)_2(DPSalH_2)^-]^{2+}$.[32] In the case of $[Ru(bpy)_3]^{2+}$ the absorption increase above 700 nm is in good agreement with earlier reports in which a broad absorption band peaking around 900 nm was assigned to a T–T transition of the MLCT excited-state species.[33] The absence of absorption changes with significant amplitude in

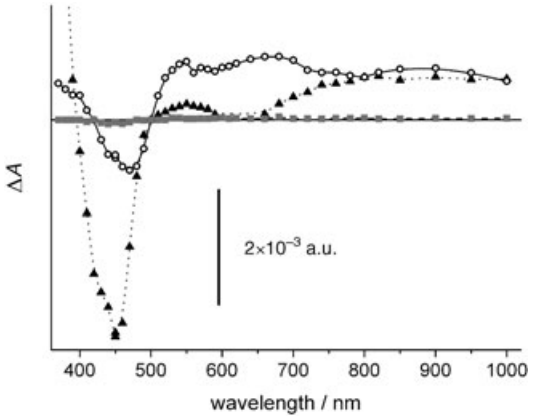

Figure 11. Spectra of flash-induced absorption changes on excitation with a nanosecond laser flash (355 nm). $[Ru(bpy)_3]$ (dotted line, triangles), $[Ru(bpy)_2(DPSalH_2)](ClO_4)_2$ (solid line, circles), $[Ru(bpy)_2(DPSalCu)](ClO_4)$ (dashed line, squares) in argon-saturated EtOH. Sample concentrations were adjusted for equal absorption at the excitation wavelength ($OD_{355} = 0.4$). Amplitudes of absorbance changes were taken about 0.5 μs after the flash and were corrected for the emission.

the case of the Ru/Cu compound indicates the absence of charge separation on the time scale of nanoseconds and longer.

If $[Ru(bpy)_2(DPSalH_2)]^{2+}$ acts as a charge-separating device with a lifetime on the order of 30 μs, it should be possible to efficiently reduce an external electron acceptor such as methyl viologen ($E(MV^{2+}/MV^{\bullet+}) = -0.45$ V versus NHE).

In Figure 12a, the kinetics of flash-induced absorption changes at 600 nm, where the reduced $MV^{\bullet+}$ absorbs, are shown in the absence and the presence of 10 mM MV^{2+}. Indeed, very efficient and long-lived (>100 μs) reduction of MV^{2+} [Eq. (1)] is observed in the case of $[Ru(bpy)_2(DPSalH_2)]^{2+}$, whereas MV^{2+} reduction was negligible for the Ru/Cu complex (not shown).

$$[Ru^{III}(bpy)_2(DPSalH_2)^{\bullet-}]^{2+} + MV^{2+} \rightarrow [Ru^{III}(bpy)_2(DPSalH_2)]^{3+} + MV^{\bullet+} \quad (1)$$

These findings confirm the interpretations given above concerning the occurrence of a long-lived charge-separated state in the former complex and its absence in the latter. In the case of $[Ru(bpy)_2(DPSalH_2)]^{2+}$, the action of MV^{2+} as electron acceptor can also be followed by measuring the absorption of the reduced ligand $[DPSalH_2]^{\bullet-}$ in the near-infrared region (Figure 12b). In the absence of methyl viologen the flash-induced absorption increase at 820 nm disappears with a half-life of about 30 μs (see inset to Figure 12), most probably following an intramolecular charge-recombination pathway, as confirmed by the similar rate of regeneration of Ru^{II} observed at 450 nm (not shown). After addition of the electron scavenger the decay at 820 nm is strongly accelerated and occurs with kinetics ($\tau \approx 2$ μs) comparable to those of reduction of MV^{2+} observed under identical conditions (Figure 12a). In addition, the absorption change at 450 nm is much faster than the decay of $MV^{\bullet+}$ (Figure 13). These observations demonstrate that the photogenerated Ru^{III} oxidant is reduced to Ru^{II} by an electron donor other than $MV^{\bullet+}$.

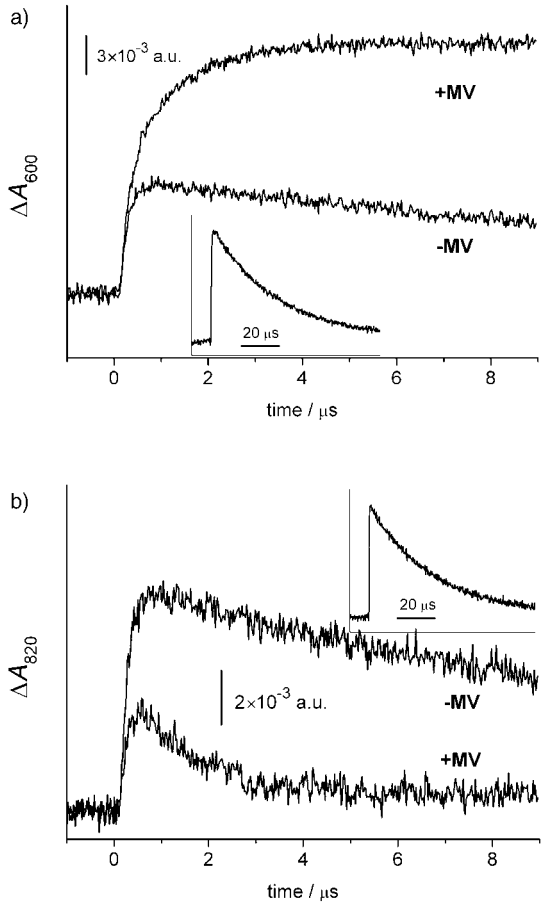

Figure 12. Time-resolved absorption changes at 600 nm (a) and 820 nm (b) upon excitation with nanosecond laser flashes at 355 nm for $[Ru(bpy)_2(DPSalH_2)](ClO_4)_2$ in the absence and presence of 10 mM MV^{2+} in argon-saturated $EtOH/H_2O$ (90/10). Insets: decay of the transient absorption in the absence of MV^{2+} on an extended time scale.

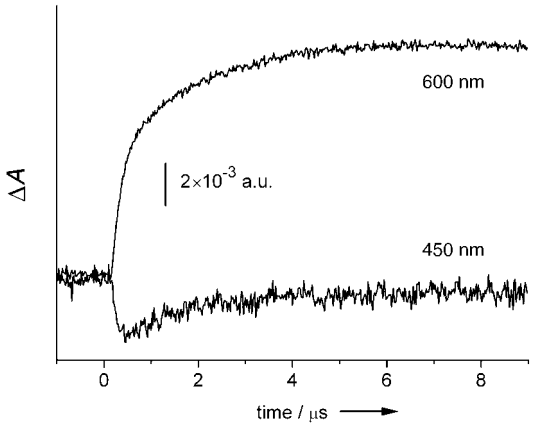

Figure 13. Time-resolved absorption changes at 600 and 450 nm on excitation with nanosecond laser flashes at 355 nm for $[Ru(bpy)_2(DPSalH_2)](ClO_4)_2$ in the presence of 10 mM MV^{2+} in argon-saturated $EtOH/H_2O$ (90/10).

Based on the electrochemical studies, we propose that the donor site responsible for the reduction of Ru^{III} is the phenol group of the ligand [Eq. (2)].

$$[Ru^{III}(bpy)_2(DPSalHArOH)]^{3+} \rightarrow [Ru^{II}(bpy)_2(DPSalHArO^{\bullet})]^{2+} + H^+ \quad (2)$$

To confirm this hypothesis, a sample of $[Ru^{II}(bpy)_2(DPSalH_2)]^{2+}$ in water/ethanol (1/1) was illuminated in the presence of an excess of the irreversible electron acceptor $[Co^{III}(NH_3)_5Cl]^{2+}$ and was rapidly frozen. The EPR spectrum of this sample displayed a narrow signal with no resolved structure (see Figure 14). The observed g_{iso} value of 2.004 is characteristic of a phenoxyl radical.

The relevant photophysical events for $[Ru(bpy)_2(DPSalH_2)]^{2+}$ are schematically depicted in Figure 15.

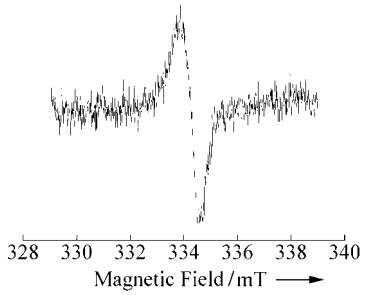

Figure 14. EPR spectra of $[Ru(bpy)_2(DPSalHArO^{\bullet})]^{2+}$ obtained after illumination of the sample in the presence of $[Co^{III}(NH_3)_5Cl]^{2+}$. Experimental conditions: $T=100$ K, $\nu_{mw}=9.37818$ GHz, amplitude modulation 0.4 mT, microwave power 16 μW, modulation frequency 100 kHz, 4 scans.

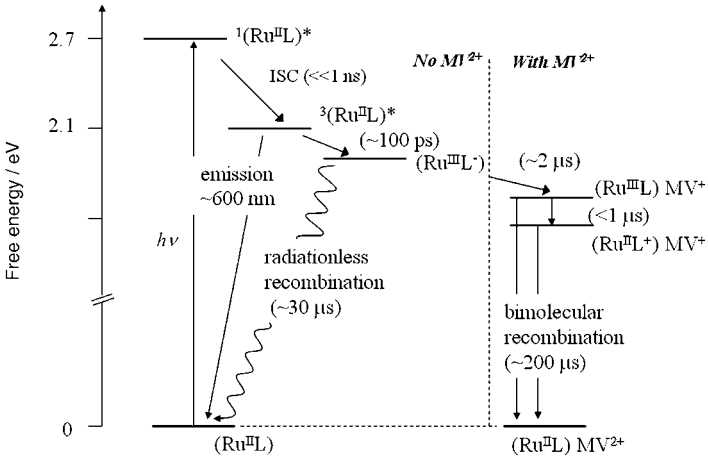

Figure 15. Schematic energy-level diagram and photophysical processes for $[Ru(bpy)_2(DPSalH_2)]^{2+}$. Reaction times are as observed under the conditions of the photophysical measurements. In the presence of 10 mM methyl viologen, the long-lived charge-separated state $Ru^{III}L^-$ (L = $DPSalH_2$) undergoes oxidative quenching by intermolecular electron transfer to yield the intermediate state $Ru^{III}L+MV^+$, which evolves by intramolecular electron transfer to the state $Ru^{II}L^+$.

Conclusion

In this first chapter of the coordination chemistry of the ditopic ligand $DPSalH_2$, we have examined the electrochemical behaviour of the ruthenium and ruthenium/copper complexes. From spectroelectrochemical studies, we have shown that the coordinated ditopic ligand is the locus for the first oxidation and reduction processes. This is the case whether the coordinating N_2O_2 cavity is metal-free or metallated. DFT calculations were also consistent with these observations. The fact that no drastic modification is observed in the redox potential of each constitutive component supports a weakly coupled system. Also, a remarkably long lived charge-separated state (>30 μs) is generated on excitation in the MLCT band for the $[Ru(bpy)_2(DPSalH_2)]^{2+}$ complex. A phenoxyl radical was characterised after illumination of this complex in the presence of $[Co^{III}(NH_3)_5Cl]^{2+}$.

Within the time resolution of our apparatus no electron transfer was observed for $[Ru(bpy)_2(DPSalCu)]^{2+}$. To elucidate this issue, faster photophysical studies (femtosecond time scale) will be necessary. With the aim of unravelling the electronic modification of the $Ru(bpy)_3^{2+}$ lumophore by the copper ion, we are performing DFT calculations on both ruthenium-containing complexes.

Experimental Section

Electrochemical measurements were made with an EGG PAR (model 273 A) electrochemical workstation. The solvents were distilled under nitrogen in the presence of dry calcium chloride, and the solutions (1 mmol L^{-1} for complexes and ligand and 0.1 mol L^{-1} of tetrabutylammonium perchlorate ($TBAClO_4$)) introduced into an argon-purged heart-shaped cell. Cyclic voltammetry was performed with a glassy carbon electrode (3 mm in diameter) as working electrode, a platinum grid as counterelectrode and an $Ag/AgClO_4$ (0.01 M) electrode in acetonitrile as reference ($E_{ref}=0.3$ V/SCE). Electrolyses were carried out at controlled potentials in a three-electrode cell with a platinum gauze as working electrode, a platinum grid as counterelectrode and an $Ag/AgClO_4$ (0.01 M) electrode in acetonitrile as reference. Low-temperature electrolyses were run with 0.2 M of $TBAClO_4$. UV/Vis/NIR spectra were recorded with a Varian Cary 5E spectrophotometer (200–1500 nm) in 1 cm quartz cells. Spectroelectrochemical data were obtained by using a three-electrode thin cell (0.5 mm) mounted in a UV/Vis/NIR spectrophotometer. IR spectra were recorded with a Perkin-Elmer spectrum 1000 spectrometer on KBr-matrix pellets. NMR spectra in $CDCl_3$ or $[D_6]$DMSO were obtained with Bruker AC 200 (200 MHz) and AC 250 (250 MHz) spectrometers. EPR spectra were recorded on a X-band spectrometer Elexsys E500 (Bruker) at 15, 77 or 100 K. Elemental analyses were performed at Services de Microanalyse, ICSN-CNRS, Gif-sur-Yvette. Mass spectra were recorded on a Finnigan Mat, Mat95S in a BE configuration at low resolution.

All theoretical calculations were carried out using Becke's three-parameter hybrid functional[24] with the LYP correlation functional of Lee, Yang and Parr[25] (B3LYP), as implemented in the Gaussian 98 package.[26] For the open-shell system DPSalCu, calculations were unrestricted (UB3LYP). A LanL2DZ effective core potential basis set[27] was employed for all atoms. Geometry optimisations were performed in C_2 symmetry (C_{2v} for phenanthroline) with the phenanthroline and phenol rings kept planar. All other internal coordinates were varied except the C–H distances.

Flash absorption and emission transients were measured with setups of local design. All measurements were done at 296 K. For absorption transients the measuring light was provided by a 150 W tungsten–halogen lamp. The wavelength was selected with interference filters placed before and a monochromator (Czerny-Turner) placed after the 10×10 mm sealed cuvette containing the sample. The sample was excited at 90° to the measuring beam by a flash from a frequency-tripled Nd:YAG laser (355 nm, duration 5 ns, ca. 6 mJ cm^{-2}; Surelight, Continuum). Absorbance changes were detected with a silicon photodiode and signals were amplified by a wideband preamplifier (model 5185, EG&G) before recording by a digital oscilloscope (TDS 3034B, Tektronix). For emission transients excitation was done by a flash from a frequency-doubled picosecond Nd:YAG laser (532 nm, duration 25 ps, ca. 300 μJ cm^{-2}; Continuum) or from a frequency-doubled nanosecond Nd:YAG laser (532 nm, duration 7 ns, 2 mJ cm^{-2}; Quantel). The detection wavelength was selected by interference filters and signals detected with a microchannel-plate photomultiplier tube (R2566U, Hamamatsu) and a 7 GHz digitising oscilloscope (IN7000, Intertechnique) or by a digital oscilloscope (TDS 744 A, Tektronix).

Ruthenium trichloride was purchased from Aldrich Chemical Company. 2,2′-Bipyridine (bpy) and 1,10-phenanthroline (phen) were obtained from Janssen Chemical Company. 1,10-phenanthroline-5,6-diamine (**1**),[28] 3,5-

di-*tert*-butylsalicylaldehyde (**2**),[29] $[Ru(bpy)_2Cl_2]$[30] and $SalH_2$[31] were synthesised as described in the literature.

Synthesis of $DPSalH_2$: 1,10-Phenanthroline-5,6-diamine (**1**, 200 mg, 0.95 mmol) and 3,5-diterbutylsalicylaldehyde (**2**, 670 mg, 2.86 mmol) were suspended in dry ethanol (30 mL) together with a few drops of triethyl orthoformate. The mixture was heated to reflux for 2 h, and the yellow precipitate collected by filtration, washed with diethyl ether and dried under vacuum. Yield 81%; elemental analysis calcd (%) for $C_{42}H_{50}N_4O_2$ (642.87): C 78.47, H 7.84, N 8.72, O 4.98; found: C 76.21, H 7.95, N 7.83. ^{1}H NMR ($CDCl_3$): $\delta = 13.15$ (s, 2H), 9.18 (dd, 2H), 8.71 (s, 2H), 8.42 (dd, 2H), 7.63 (dd, 2H), 7.45 (d, 2H), 7.11 (d, 2H), 1.45 (s, 18H), 1.25 ppm (s, 18H); IR: $\tilde{\nu} =$ 3451.5 (OH), 2964.23, 2909.24, 2871.20 (CH), 1614.18 (C=N phen), 1571.30 cm^{-1} (C=N imine).

Synthesis of $[Ru(bpy)_2(DPSalH_2)](ClO_4)_2$: *cis*-$[Ru(bpy)_2Cl_2]\cdot 2H_2O$ (30 mg, 0.057 mmol) and $AgNO_3$ (19.6 mg, 0.115 mmol) were suspended in methanol (5 mL). The mixture was stirred magnetically for 1 h under an argon atmosphere and the white precipitate of AgCl was filtered off. $DPSalH_2$ (37 mg, 0.051 mmol) dissolved in dichloromethane was added to the clear red solution followed by a few drops of triethyl orthoformate. The reaction mixture was heated to reflux in the dark with stirring under argon for 2 h. The reddish solution was then concentrated on a rotatory evaporator. An orange solid precipitated on addition of a concentrated aqueous solution of $NaClO_4$. The precipitate was collected by filtration and washed with water. Yield 84%; elemental analysis calcd (%) for $C_{62}H_{66}Cl_2N_8O_{10}Ru\cdot 0.5\,NaClO_4$ (1316.43): C 56.57, H 5.05, N 8.51; found: C 56.31, H 5.09, N 8.50. ^{1}H NMR ([D_6]DMSO): $\delta = 12.89$ (s, 2H), 9.06 (s, 2H), 8.87 (t, 4H), 8.65 (d, 2H), 8.15 (m, 6H), 7.85 (m, 4H), 7.63 (m, 4H), 7.4 (m, 6H), 1.34 (s, 18H), 1.22 ppm (s, 18H); IR: $\tilde{\nu} =$ 3423.68 (OH), 2954.42, 2867.38 (CH), 1615.76 (C=N phen), 1584.76 (C=N imine), 1087.69 cm^{-1} (ClO_4).

Synthesis of $[Ru(bpy)_2(DPSalCu)](ClO_4)_2$: $[Ru(bpy)_2(DPSalH_2)](ClO_4)_2$ (50 mg, 0.04 mmol) was dissolved in methanol (20 mL) and Cu(acetate)$_2\cdot H_2O$ (10 mg, 0.05 mmol) was added. The mixture was stirred at room temperature overnight. The deep red solution was concentrated under reduced pressure and a solid precipitated on addition of a concentrated aqueous solution of $NaClO_4$. The red solid was filtered off, washed with water and dried under vacuum. Yield 82%; ES-MS: m/z 558.7 [M^{2+}]; IR: $\tilde{\nu} =$2951.55, 2901.96, 2868.34 (CH), 1616.78 (C=N phen), 1571.30 (C=N imine), 1087.68 cm^{-1} (ClO_4).

Synthesis of SalCu: $SalH_2$ (60 mg, 0.11 mmol) was dissolved in methanol (20 mL) and Cu(acetate)$_2\cdot H_2O$ (25 mg, 0.125 mmol) was added. The mixture was heated to reflux for 3 h. A red powder precipitated and was filtered off, washed with methanol and water and dried under vacuum. Yield 86%; ES-MS: m/z 602.3 [M^+]; IR: $\tilde{\nu} =$2953.65, 2906.50, 2867.44 (CH), 1605.56 cm^{-1} (C=N).

Acknowledgement

This work was supported by the CNRS (Programme Energie, PRI4), the CEA for the LRC project (LRC-CEA n°33V) and STREP SOLAR-H 516510. A.Q. acknowledges the European Commission for financial support (Contract "WONDERFUL", HPRN-CT-2002-00177). We thank the Centre Informatique National de l'Enseignement Supérieur at Montpellier (France) and the Institut du Développement et des Ressources en Informatique Scientifique at Orsay (France) for providing calculation means.

[1] a) K. Kalyanasundaram, *Coord. Chem. Rev.* **1982**, *46*, 159–244; b) A. Juris, V. Balzani, F. Barigelletti, S. Campagna, P. Belser, A. von Zelewsky, *Coord. Chem. Rev.* **1988**, *84*, 85–277; c) A. Juris, V. Balzani, *Coord. Chem. Rev.* **2001**, *211*, 97–115.

[2] a) V. Balzani, P. Ceroni, M. Maestri, V. Vicinelli, *Curr. Opin. Chem. Biol.* **2003**, *7*, 657–665; b) S. Campagna, C. Di Pietro, F. Loiseau, B. Maubert, N. McClenaghan, R. Passalacqua, F. Puntotiero, V. Ricevuto, S. Serroni, *Coord. Chem. Rev.* **2003**, *229*, 67–74.

[3] a) J. Otsuki, M. Tsujino, T. Lizaki, K. Araki, M. Seno, K. Takatera, T. Watanabe, *J. Am. Chem. Soc.* **1997**, *119*, 7895–7896; b) S. Fraysse, C. Coudret, J.-P. Launay, *Eur. J. Inorg. Chem.* **2000**, 1581–1590; c) J. M. Serin, D. W. Brousmiche, J. M. J. Fréchet, *J. Am. Chem. Soc.* **2002**, *124*, 11848–11849; d) S. Welter, K. Brunner, J. W. Hofstraat, L. DeCola, *Nature* **2003**, *421*, 54–57.

[4] a) A. R. Dunn, I. J. Dmochowski, J. R. Winkler, H. B. Gray, *J. Am. Chem. Soc.* **2003**, *125*, 12450–12456; b) F. Scandola, C. Chiorboli, M. T. Indelli, M. A. Rampi, *Electron Transfer in Chemistry*, *Vol. 3*, (Ed.: V. Balzani), Wiley-VCH, Weinheim, **2001**, pp. 337–408, and references therein.

[5] a) A. Beyeler, P. Belser, *Coord. Chem. Rev.* **2002**, *230*, 29–39, and references therein; b) R. Ziessel, M. Hissler, A. El-ghayoury, A. Harriman, *Coord. Chem. Rev.* **1998**, *177*, 1251–1298.

[6] M. N. Paddon-Row, *Electron Transfer in Chemistry*, *Vol. 3* (Ed.: V. Balzani), Wiley-VCH, **2001**, pp. 179–271, and references therein.

[7] C. Kaes, A. Katz, M. W. Hosseini, *Chem. Rev.* **2000**, *100*, 3553–3590, and references therein.

[8] L. Sun, L. Hammarström, B. Akermark, S. Styring, *Chem. Soc. Rev.* **2001**, *30*, 36–49, and references therein.

[9] a) N. Kitamura, H.-B. Kim, S. Sumio, S. Tazuke, *J. Phys. Chem.* **1989**, *93*, 5750–5756; b) H.-B. Kim, N. Kitamura, Y. Kawanishi, S. Tazuke, *J. Phys. Chem.* **1989**, *93*, 5757–5764; c) M. Kirch, J. M. Lehn, J. P. Sauvage, *Helv. Chim. Acta* **1979**, *62*, 1345–1384.

[10] Y. Pellegrin, K. E. Berg, G. Blondin, E. Anxolabéhère-Mallart, W. Leibl, A. Aukauloo, *Eur. J. Inorg. Chem.* **2003**, 1900–1910.

[11] K. K. Chatterjee, N. Farrier, B. E. Douglas, *J. Am. Chem. Soc.* **1963**, *85*, 2919–2922.

[12] K. Nakamoto, *Infrared and Raman Spectra of Inorganic and Coordination Compounds*, 5th Ed., Wiley, New York, **1997**.

[13] a) S. D. Ernst, W. Kaim, *Inorg. Chem.* **1989**, *28*, 1520–1528; b) E. Ishow, A. Gourdon, J. P. Launay, C. Chiorboli, F. Scandola, *Inorg. Chem.* **1999**, *38*, 1504–1410; c) L. Flamigni, S. Encinas, F. Barigelletti, F. M. MacDonnell, K-J. Kim, F. Puntoriero, S. Campagna, *Chem. Commun.* **2000**, 1185–1186; d) M.-J. Kim, R. Konduri, H. Ye, F. M. MacDonnell, F. Puntoriero, S. Serroni, S. Campagna, T. Holder, G. Kinsel, K. Rajeshwar, *Inorg. Chem.* **2002**, *41*, 2471–2476.

[14] a) A. H. Maki, B. R. McGarvey, *J. Chem. Phys.* **1958**, *29*, 35–38; b) M. M. Bhadbhade, D. Srinivas, *Inorg. Chem.* **1993**, *32*, 5458–5466.

[15] M. Iwaizumi, T. Kudo, S. Kita, *Inorg. Chem.* **1986**, *25*, 1546–1550.

[16] a) J. Müller, K. Felix, C. Maidile, E. Lengfelder, J. Strähle, U. Weser, *Inorg. Chim. Acta* **1995**, *233*, 11–19; b) U. Sakagachi, A. W. Addison, *J. Chem. Soc. Dalton Trans.* **1979**, 600–608.

[17] M. Venturi, A. Credi, V. Balzani, *Coord. Chem. Rev.* **1999**, *185–186*, 233–256, and references therein.

[18] M. N. Ackermann, L. V. Interrante, *Inorg. Chem.* **1984**, *23*, 3904–3911.

[19] R. C. Pratt, T. D. P. Stack, *J. Am. Chem. Soc.* **2003**, *125*, 8716–8717.

[20] a) P. Chaudhuri, M. Hess, T. Weyhermuller, K. Wieghardt, *Angew. Chem.* **1999**, *111*, 1165–1168; *Angew. Chem. Int. Ed.* **1999**, *38*, 1095–1098; b) P. Chaudhuri, M. Hess, J. Müller, K. Hildenbrand, E. Bill, T. Weyhermuller, K. Wieghardt, *J. Am. Chem. Soc.* **1999**, *121*, 9599–9610.

[21] N. Komatsuzaki, Y. Himeda, M. Goto, K. Kasuga, H. Sugihara, H. Arakawa, *Chem. Lett.* **1999**, 327–328.

[22] T. Ziegler, *Chem. Rev.* **1991**, *91*, 651–667.

[23] a) N. H. Damrauer, G. Cerullo, A. Yeh, T. R. Boussie, C. V. Shank, J. K. McCusker, *Science* **1997**, *275*, 54–57; b) A. T. Yeh, C. V. Shank, J. K. McCusker, *Science* **2000**, *289*, 935–938.

[24] A. D. Becke, *J. Chem. Phys.* **1993**, *98*, 5648–5652.

[25] C. Lee, W. Yang, R. G. Parr, *Phys. Rev. B* **1988**, *37*, 785–789.

[26] Gaussian 98, Revision A.11, M. J. Frisch, G. W. Trucks, H. B. Schlegel, G. E. Scuseria, M. A. Robb, J. R. Cheeseman, V. G. Zakrzewski, J. A. Montgomery, Jr., R. E. Stratmann, J. C. Burant, S. Dapprich, J. M. Millam, A. D. Daniels, K. N. Kudin, M. C. Strain, O. Farkas, J. Tomasi, V. Barone, M. Cossi, R. Cammi, B. Mennucci, C. Pomelli, C. Adamo, S. Clifford, J. Ochterski, G. A. Petersson, P. Y. Ayala, Q. Cui, K. Morokuma, P. Salvador, J. J. Dannenberg, D. K. Malick, A. D. Rabuck, K. Raghavachari, J. B. Foresman, J. Cioslowski, J. V.

Ortiz, A. G. Baboul, B. B. Stefanov, G. Liu, A. Liashenko, P. Piskorz, I. Komaromi, R. Gomperts, R. L. Martin, D. J. Fox, T. Keith, M. A. Al-Laham, C. Y. Peng, A. Nanayakkara, M. Challacombe, P. M. W. Gill, B. Johnson, W. Chen, M. W. Wong, J. L. Andres, C. Gonzalez, M. Head-Gordon, E. S. Replogle, and J. A. Pople, Gaussian, Inc., Pittsburgh PA, **2001**.

[27] a) T. H. Dunning, Jr., P. J. Hay in *Modern Theoretical Chemistry*, *Vol. 3* (Ed.: H. F. Schaefer III), Plenum, New York, **1976**, pp. 1–28; b) P. J. Hay, W. R. Wadt, *J. Chem. Phys.* **1985**, *82*, 270–283.

[28] S. Bodige, F. M. MacDonnell, *Tetrahedron Lett.* **1997**, *38*, 8159–8160.

[29] J F. Larrow, E. N. Jacobsen, Y. Gao, Y. Hong, X. Nie, C. M. Zepp, *J. Org. Chem.* **1994**, *59*, 1939–1942.

[30] B. P. Sullivan, T. J. Meyer, *Inorg. Chem.* **1978**, *17*, 3334–3341.

[31] R. Paschke, D. Balkow, E. Sinn, *Inorg. Chem.* **2002**, *41*, 1949–1953.

[32] Formation of solvated electron can be excluded. See Supporting Information.

[33] a) K. Miedlar, P. K. Das, *J. Am. Chem. Soc.* **1982**, *104*, 7462–7469; b) O. Shimizu, J. Watanabe, S. Naito, *Chem. Phys. Lett.* **2000**, *332*, 295–298.

Received: October 19, 2004
Published online: April 5, 2005